MUSIC imaging method for electromagnetic inspection of composite multi-layers

Giacomo Rodeghiero, Ping-Ping Ding, Yu Zhong, Marc Lambert, Dominique Lesselier

This is the last version (before editor's corrections) of G. Rodeghiero et al. (2015). "MUSIC imaging method for electromagnetic inspection of composite multi-layers". *Review of Progress in Quantitative Nondestructive Evaluation*. Vol. 1650. 1. Plenum Press, pp. 453–461. DOI: 10.1063/1.4914641. URL: https://doi.org/10.1063/1.4914641

MUSIC imaging method for electromagnetic inspection of composite multi-layers

Giacomo Rodeghiero[1], Ping-Ping Ding[1], Yu Zhong[2], Marc Lambert[1], and Dominique Lesselier[1]

[1]Département de Recherche en Électromagnétisme, Laboratoire des Signaux et Systèmes UMR8506 (CNRS–SUPELEC–Univ. Paris-Sud)
[2]A*STAR, Institute of High Performance Computing, Singapore

Abstract

A first-order asymptotic formulation of the electric field scattered by a small inclusion (with respect to the wavelength in dielectric regime or to the skin depth in conductive regime) embedded in composite material is given. It is validated by comparison with results obtained using a Method of Moments (MoM). A non-iterative MUltiple SIgnal Classification (MUSIC) imaging method is utilized in the same configuration to locate the position of small defects. The effectiveness of the imaging algorithm is illustrated through some numerical examples.

1 Introduction

Non-destructive Testing-Evaluation (NdT-E) of damaged multi-layer structures like fiber-made composite materials involved in aeronautic and automotive industries is a topic of great interest to solve problems of viability and security.

From eddy currents to test graphite-based materials to microwaves and beyond to test glass-based composite structures, one aims to obtain images of the possibly damaged parts with robust, fast inversion algorithms. In this contribution, such algorithms are tailored to detect small (compared to the local wavelength in propagative regime or skin depth in diffusive regime) inclusions affecting the structures mentioned above. These inclusions may be voids, fluid-filled cavities (i.e., isotropic) or even uniaxial ones. Yet this requires proper models of the layerings to compute their response due to electromagnetic sources, notably electric dipoles.

Based on (Zhong, Lambert, et al. 2014), it is proposed herein a method to compute in an effective fashion the dyadic Green's functions (DGF) in the spectral domain for such structures within the framework of contrast-source integral equations. When the sources are far away from the origin, the spectrum of the DGF can be fast-oscilltaing. Therefore, in order to compute in an efficent manner its inverse Fourier transform, the Padua-Domínguez interpolation-integration technique is exploited (Caliari et al. 2011; Domínguez, Graham, and Smyshlyaev 2011). A first-order solution of the forward problem involving possibly anisotropic defects described by the so-called depolarization tensor (Sihvola 2005; Weiglhofer and Lakhtakia 1996) will be presented and the results obtained will be compared to those provided by a Method of Moments (MoM) described in (Zhong, Ding, et al. 2014).

The well-known MUltiple SIgnal Classification (MUSIC) imaging method described in (Ammari et al. 2007; Iakovleva et al. 2007; Henriksson, Lambert, and Lesselier 2011), which uses such DGF, is here applied to retrieve the position of small defects embedded in glass-epoxy composite laminate (Teo, Wang, and Chiu 2006). The main drawback of MUSIC is its sensitiveness with respect to the noise, which perturbs the resolution of the imaging method giving not good results. The introduction of MUSIC with enhanced resolution (Chen and Zhong 2009) will overcome such a problem, providing quality results in presence of noise.

2 Method

The time-harmonic dependence $e^{-i\omega t}$ is assumed and dropped, all the calculations being carried at a single angular frequency ω. For a vector $\mathbf{r} = (x, y, z)$, $r = |\mathbf{r}|$. Let us consider the physical scenario sketched in Fig. 1

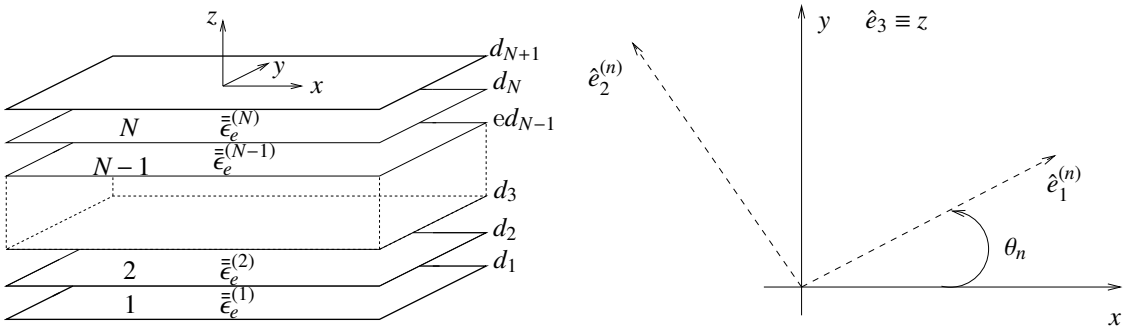

Fig. 1: Geometry of the general planar multilayered composite medium (left). The local and global coordinate systems (right).

(left), where a complex, multi-layer structure is depicted. Each n layer, ($n = 1, \cdots, N$), is assumed non-magnetic ($\mu = \mu_0$) homogeneous uniaxial, with different dielectric properties from one layer to the next. In the local coordinate system (material frame), which is formed by the three mutually orthogonal axes $\hat{e}_1^{(n)}$, $\hat{e}_2^{(n)}$, and $\hat{e}_3^{(n)} \equiv z$, each layer is characterized by a diagonal (complex-valued) permittivity tensor which reads as

$$\bar{\bar{\epsilon}}_e^{(n)} = \begin{bmatrix} \epsilon_{11}^{(n)} & 0 & 0 \\ 0 & \epsilon_{22}^{(n)} & 0 \\ 0 & 0 & \epsilon_{22}^{(n)} \end{bmatrix}, \tag{1}$$

in harmony with the uniaxial hypothesis. Thanks to the rotation transformation matrix

$$\bar{\bar{\Xi}}(\theta_n) = \begin{bmatrix} \cos\theta_n & \sin\theta_n & 0 \\ -\sin\theta_n & \cos\theta_n & 0 \\ 0 & 0 & 1 \end{bmatrix} \tag{2}$$

and its inverse

$$\bar{\bar{\Xi}}^{-1}(\theta_n) = \begin{bmatrix} \cos\theta_n & -\sin\theta_n & 0 \\ \sin\theta_n & \cos\theta_n & 0 \\ 0 & 0 & 1 \end{bmatrix}, \tag{3}$$

one is able to carry the local coordinate system to the global Cartesian one. The two matrices are functions of the rotation Euler angle θ_n, as represented in Fig. 1 (right).

It is possible to compute the electromagnetic response of the structure sketched in Fig. 1 with the eigenvalue analysis of the so-called propagator matrix as presented in (Zhong, Lambert, et al. 2014) and references therein. In particular, given the position $\mathbf{r}$ of a known excitation source (with polarization $\boldsymbol{\beta}$) in the n-th layer ($n = 1, \cdots, N$), one is able to compute the electromagnetic fields at a position $\mathbf{r}'$ in the q-th layer ($q = 1, \cdots, N$). One consequently obtains the dyadic Green's function $\bar{\bar{G}}(\mathbf{r}, \mathbf{r}')$ from the source position $\mathbf{r}$ in the n-th layer to the observation point $\mathbf{r}'$ in the q-th layer. Since one is considering non-magnetic media, the equality

$$\bar{\bar{G}}(\mathbf{r}, \mathbf{r}') = \left(\bar{\bar{G}}(\mathbf{r}', \mathbf{r})\right)^T \tag{4}$$

is true (Iakovleva et al. 2007), T stands for the transpose. $\bar{\bar{G}}(\mathbf{r}, \mathbf{r}')$ is the solution of the equation

$$\nabla \times \nabla \times \bar{\bar{G}}(\mathbf{r}, \mathbf{r}') - k^2 \bar{\bar{G}}(\mathbf{r}, \mathbf{r}') = \bar{\bar{I}}\delta(\mathbf{r} - \mathbf{r}'), \tag{5}$$

which satisfies the radiation condition at infinity (the Sommerfeld condition) and in a complex multi-layer continuity conditions at each interface. In this contribution, one refers to the electric-electric dyadic Green's function $\bar{\bar{G}}^{\mathrm{ee}}(\mathbf{r}, \mathbf{r}')$ to compute the electric field in $\mathbf{r}'$ due to an elementary electric dipole in $\mathbf{r}$ with current density $\mathbf{J}_0(\mathbf{r}) = \boldsymbol{\beta} Il\delta(\mathbf{r} - \mathbf{r}')$, where the constant Il is the current moment.

If an inclusion with permittivity tensor $\bar{\bar{\epsilon}}_i$ and volume V affects the background medium, the difference between the total electric field in the presence of the inclusion $\mathbf{E}^{\mathrm{tot}}(\mathbf{r})$ and the field without the presence of the inclusion $\mathbf{E}^{\mathrm{inc}}(\mathbf{r})$ gives the scattered field $\mathbf{E}^{\mathrm{sca}}(\mathbf{r})$. The integral equation which follows is the Lippman-Schwinger one

$$\mathbf{E}^{\mathrm{sca}}(\mathbf{r}) = \mathrm{i}\omega\mu_0 \int_V \bar{\bar{G}}^{\mathrm{ee}}(\mathbf{r}, \mathbf{r}') \cdot \bar{\bar{\chi}}(\mathbf{r}') \cdot \mathbf{E}^{\mathrm{tot}}(\mathbf{r}')\, \mathrm{d}\mathbf{r}', \tag{6}$$

where

$$\bar{\bar{\chi}}(\mathbf{r}) = -\mathrm{i}\omega\epsilon_0 \bar{\bar{\Xi}}^{-1}(\theta_n) \cdot \left(\bar{\bar{\epsilon}}_i - \bar{\bar{\epsilon}}_e^{(n)}\right) \cdot \bar{\bar{\Xi}}(\theta_n) \tag{7}$$

is the contrast function. The incident field is defined as

$$\begin{aligned} \mathbf{E}^{\mathrm{inc}}(\mathbf{r}) &= \mathrm{i}\omega\mu_0 \int \bar{\bar{G}}^{\mathrm{ee}}(\mathbf{r},\mathbf{r}') \cdot \mathbf{J}_0(\mathbf{r}')\,\mathrm{d}\mathbf{r}' \\ &= \mathrm{i}\omega\mu_0 \bar{\bar{G}}^{\mathrm{ee}}(\mathbf{r},\mathbf{r}') \cdot \boldsymbol{\beta} I l, \end{aligned} \tag{8}$$

since one assumes the source as elementary.

2.1 Asymptotic formula of the scattered field in stratified media

If one considers that the inclusion mentioned above is characterized by a diagonal permittivity tensor $\bar{\bar{\epsilon}}_i = \bar{\bar{I}}\epsilon_i$ and it is small with respect to the wavelength of the free-space, equation (6) can be simplified into the so-called asymptotic formulation of the scattered field, which reads as

$$\mathbf{E}^{\mathrm{sca}}(\mathbf{r}) = \mathrm{i}\omega\mu_0 \bar{\bar{G}}^{\mathrm{ee}}(\mathbf{r},\mathbf{r}_m) \cdot \bar{\bar{\varrho}} \cdot \mathbf{E}^{\mathrm{inc}}(\mathbf{r}_m); \tag{9}$$

$\mathbf{r}_m$ is the position of the inclusion. The polarization tensor $\bar{\bar{\varrho}}$ for an inclusion with volume V is defined as

$$\bar{\bar{\varrho}} = -\mathrm{i}\omega\epsilon_0 V \bar{\bar{\Xi}}^{-1}(\theta_n) \cdot \begin{bmatrix} \alpha_l & 0 & 0 \\ 0 & \alpha_t & 0 \\ 0 & 0 & \alpha_t \end{bmatrix} \cdot \bar{\bar{\Xi}}(\theta_n), \tag{10}$$

where its longitudinal and tangential components read as

$$\alpha_l = \epsilon_{11}^{(n)} \frac{\epsilon_i - \epsilon_{11}^{(n)}}{\epsilon_{11}^{(n)} + L_l\left(\epsilon_i - \epsilon_{11}^{(n)}\right)} \tag{11}$$

and

$$\alpha_t = \epsilon_{22}^{(n)} \frac{\epsilon_i - \epsilon_{22}^{(n)}}{\epsilon_{22}^{(n)} + L_t\left(\epsilon_i - \epsilon_{22}^{(n)}\right)}, \tag{12}$$

respectively (Sihvola 2005). For a cubic inclusion of side a and volume $V = a^3$, $L_l = c\arctan\left(c \,/\, \sqrt{1+2c}\right)$ et $L_l + 2L_t = 1$, where $c = \epsilon_{11}^{(n)} / \epsilon_{22}^{(n)}$ (Weiglhofer and Lakhtakia 1996).

2.2 The Padua-Domínguez interpolation-integration technique

To calculate the spatial Green's function $\bar{\bar{G}}^{\mathrm{ee}}(\mathbf{r},\mathbf{r}_m)$, it is inevitable to process a time-consuming two-dimensional inverse Fourier transform of its spectral response. In this paper, one employs the Padua-Domínguez interpolation-integration technique to reduce the computational cost.

The spectral response of a multilayered structure due to a source placed at (x_s, y_s) is assumed to be written as

$$\tilde{\eta}(\xi_1,\xi_2) = \tilde{\eta}_0(\xi_1,\xi_2)\mathrm{e}^{-\mathrm{i}(\xi_1 x_\mathrm{s} + \xi_2 y_\mathrm{s})}, \tag{13}$$

where $\tilde{\eta}_0(\xi_1,\xi_2)$ is the spectral response due to the source placed at the origin of the reference system and it is the stable (or, better said, the non-oscillatory part) of $\tilde{\eta}(\xi_1,\xi_2)$.

By applying the inverse Fourier transform, (13) can be written in the following form:

$$\eta(x,y) = \frac{1}{4\pi^2} \int_a^b \int_c^d \tilde{\eta}_0(\xi_1,\xi_2)\mathrm{e}^{\mathrm{i}(\xi_1 x + \xi_2 y)}\mathrm{e}^{-\mathrm{i}(\xi_1 x_\mathrm{s} + \xi_2 y_\mathrm{s})}\,\mathrm{d}\xi_1\,\mathrm{d}\xi_2 \tag{14}$$

By properly choosing the detour path along $\left(\xi_1', \xi_2'\right)$ instead of (ξ_1,ξ_2) to avoid the singularities, (14) can be recast as:

$$\eta(x,y) = \frac{1}{4\pi^2} \int_a^b \int_c^d \tilde{f}\left(\xi_1', \xi_2'\right)\mathrm{e}^{-\mathrm{i}\left(\xi_1' x_\mathrm{s} + \xi_2' y_\mathrm{s}\right)}\,\mathrm{d}\xi_1'\,\mathrm{d}\xi_2'. \tag{15}$$

where $\tilde{f}\left(\xi_1',\xi_2'\right)$ is a non-oscillatory function related to $\tilde{\eta}_0(\xi_1,\xi_2)$.

Based on the Padua point technique (Caliari et al. 2011), (15) can be approximated as

$$\eta(x,y) \simeq \frac{1}{4\pi^2}\sum_{k=0}^{\mathrm{Pad}_n}\sum_{j=0}^{k} c_{j,k-j}\left\{\int_a^b \hat{T}_j\left(\xi_1'\right)\mathrm{e}^{-\mathrm{i}\xi_1' x_\mathrm{s}}\,\mathrm{d}\xi_1'\right\}\left\{\int_c^d \hat{T}_{k-j}\left(\xi_2'\right)\times \mathrm{e}^{-\mathrm{i}\xi_2' y_\mathrm{s}}\,\mathrm{d}\xi_2'\right\} - \frac{1}{2}c_{\mathrm{Pad}_n,0}\left\{\int_a^b \hat{T}_{\mathrm{Pad}_n}\left(\xi_1'\right)\mathrm{e}^{-\mathrm{i}\xi_1' x_\mathrm{s}}\,\mathrm{d}\xi_1'\right\}\left\{\int_c^d \hat{T}_0\left(\xi_2'\right)\mathrm{e}^{-\mathrm{i}\xi_2' y_\mathrm{s}}\,\mathrm{d}\xi_2'\right\}, \tag{16}$$

where Pad_n is the Padua points degree chosen for the interpolation. Here, $\hat{T}_j$ is the scaled Chebyshev polynomial of degree j. The coefficients $c_{j,k-j}$ are computed in (Caliari et al. 2011). One term of the integrals in (16) can be written as

$$\begin{aligned}\int_a^b \hat{T}_j\left(\xi_1'\right)\mathrm{e}^{-\mathrm{i}\xi_1' x_\mathrm{s}}\,\mathrm{d}\xi_1' &= \frac{(b-a)}{2}\int_{-1}^{1}\sqrt{2}\cos\left[j\cos^{-1}\left(\xi_1'\right)\right]\mathrm{e}^{-\mathrm{i}\xi_1' x_\mathrm{s}}\,\mathrm{d}\xi_1' \\ &= \sqrt{2}\frac{(b-a)}{2}\int_{-1}^{1}\cos\left[j\cos^{-1}\left(\xi_1'\right)\right]\mathrm{e}^{-\mathrm{i}\xi_1' x_\mathrm{s}}\,\mathrm{d}\xi_1',\end{aligned} \tag{17}$$

the result of which can be obtained in (Domínguez, Graham, and Smyshlyaev 2011).

2.3 Multistatic response matrix and MUSIC imaging

Let us consider a source network, made by N_s sources at the positions $\mathbf{r}_s$, $(s=1,\cdots,N_s)$ all having the same orientation $\boldsymbol{\beta}$. N_o receiving dipoles at the positions $\mathbf{r}_o$, $(o=1,\cdots,N_o)$ form the receiver set-up. A cubic inclusion is present at $\mathbf{r}_m$. From (9), the $N_o\times N_s$ Multistatic Response matrix $\bar{\bar{A}}$ (Henriksson, Lambert, and Lesselier 2011) reads as

$$\bar{\bar{A}} = \bar{\bar{G}}^{\mathrm{ee}}(\mathbf{r}_o,\mathbf{r}_m)\cdot\bar{\bar{\varrho}}\cdot\bar{\bar{G}}^{\mathrm{ee}}(\mathbf{r}_m,\mathbf{r}_s), \tag{18}$$

with $\bar{\bar{G}}^{\mathrm{ee}}(\mathbf{r}_o,\mathbf{r}_m) = \left(\bar{\bar{G}}^{\mathrm{ee}}(\mathbf{r}_m,\mathbf{r}_s)\right)^T$. It is possible to apply the Singular Value Decomposition (SVD) on the matrix $\bar{\bar{A}}$. As a result, $\bar{\bar{A}}$ reads as

$$\bar{\bar{A}} = \bar{\bar{U}}\bar{\bar{\Sigma}}\bar{\bar{V}}^*, \tag{19}$$

where $*$ denotes transpose conjugation. Depending upon the rank of the matrices $\bar{\bar{G}}^{\mathrm{ee}}(\mathbf{r}_o,\mathbf{r}_m)$ and $\bar{\bar{G}}^{\mathrm{ee}}(\mathbf{r}_m,\mathbf{r}_s)$ (Ammari et al. 2007), the matrix $\bar{\bar{\Sigma}}$ will have s non-zero singular values. For a dielectric inclusion, the number of non-zero singular values is $s=3$. The right and left orthogonal projections on the noise sub-space are defined as

$$\mathcal{P}_r = \bar{\bar{I}} - (U_s U_s^*) \tag{20}$$

and

$$\mathcal{P}_l = \bar{\bar{I}} - (V_s V_s^*), \tag{21}$$

respectively. U_s and V_s denote the s columns of the matrices $\bar{\bar{U}}$ and $\bar{\bar{V}}$ and they form the signal subspace. The estimation function $\mathbf{W}(\mathbf{x})$ which has a peak when the test position point $\mathbf{x}$ is the same as the position of the inclusion $\mathbf{r}_m$ is defined as

$$\mathbf{W}(\mathbf{x}) = \frac{1}{\left\|\mathcal{P}_l\left(\bar{\bar{G}}^{\mathrm{ee}}(\mathbf{x},\mathbf{r}_s)\right)\cdot\mathbf{a}\right\|^2}, \tag{22}$$

with $\mathbf{a}=[1,1,1]^T$ (Ammari et al. 2007) is a proper value to choose. The vector $\mathbf{a}$ might be seen as the direction of an electric dipole induced at the test position $\mathbf{x}$.

2.3.1 MUSIC with enhanced resolution

The standard MUSIC algorithm seen above relies on the analysis of the singular values projected in the noise subspace. When the measured scattered field is contaminated by some noise, which is often the case in real-life applications, the performances of the presented imaging algorithm drop inevitably. One needs to find an optimal test dipole direction $\mathbf{a}$ also. In the studies carried on in (Chen and Zhong 2009), one chooses the optimal direction $\mathbf{a}_{\text{test}}$ as

$$\mathbf{a}_{\text{test}} = \text{argmax}_{\mathbf{a}} \frac{\sum_{i=1}^{L} \left| \mathbf{u}_i^* \cdot \bar{\bar{G}}^{\text{ee}}(\mathbf{x}, \mathbf{r}_s) \cdot \mathbf{a} \right|^2}{\left| \bar{\bar{G}}^{\text{ee}}(\mathbf{x}, \mathbf{r}_s) \cdot \mathbf{a} \right|^2}, \tag{23}$$

where L is the total number of dominant singular values, *i.e.*, those which are not too much corrupted by the noise. $\mathbf{u}_i$ is the $i-$th $(i = 1, 2, \cdots L)$ column of the matrix $\bar{\bar{U}}$, *i.e.*, its $i-$th eigenvector. The estimation function with enhanced resolution will therefore read as

$$\mathbf{W}(\mathbf{x}) = \frac{1}{1 - \sum_{i=1}^{L} \left| \mathbf{u}_i^* \cdot \bar{\bar{G}}^{\text{ee}}(\mathbf{x}, \mathbf{r}_s) \cdot \mathbf{a}_{\text{test}} \right|^2}. \tag{24}$$

3 Numerical results

This section is to investigate and discuss the accuracy of the proposed method for electromagnetic scattering problems. First, the scattered field computed with the asymptotic formulation will be compared with the one obtained by a Method of Moments (MoM) (Zhong, Ding, et al. 2014). Then, one compares the results obtained with the standard MUSIC method with those obtained with the enhanced resolution in the presence of an additive white Gaussian noise (AWGN) for detecting and locating a given number of scatters inside the region of interest.

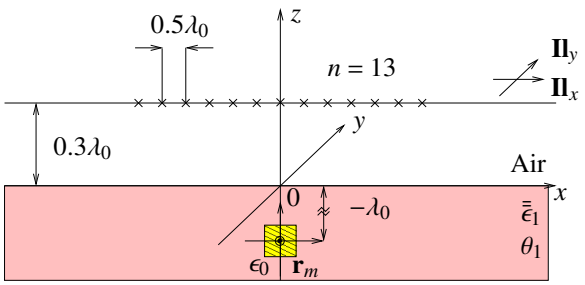

Fig. 2: Configuration set-up for the scattered field.

The study involves a half-space glass-fiber composite material shown in Fig. 2. The operating frequency in the free space is 6 GHz. The relative permittivity along the principle axis of the anisotropic medium is $\bar{\bar{\epsilon}}_1 = \text{diag}[5.46 + \text{i}2.29, 5.21 + \text{i}2.08, 5.21 + \text{i}2.08]$ with the rotation angle $\theta_1 = 0°$ with respect to the x axis. The scatterer is an air cube of side $0.1\lambda_0$, placed at $\mathbf{r}_m = (0, 0, -\lambda_0)$. λ_0 is the wavelength in free space. An array made of $N_s = N_o = 13$ electric dipoles polarized along the $x-y$ axes illuminates the half-space from $0.3\lambda_0$ height with respect to the origin of the reference system.

Figs. 3 and 4 show the scattered field collected by the receivers when the central dipole illuminates the scenario. The solid lines represent the scattered field obtained with the asymptotic formula, while the reference results obtained by the method of moments (MoM) are represented by the discrete points. It can be observed that the results based on the proposed method are in good agreement with the MoM-based results.

For MUSIC in order to have good resolution for the images one improves the transmitting-receiving network as represented in Fig. 5. The array is now made of 7×7 transceivers, covering a square surface of side $6\lambda_0$ centered at the origin of the $x-y$ plane. The lift-off is the same as before. One assumes that two air-cube inclusions are present inside a cubic research domain of side $2\lambda_0$, extending from $z = -0.25\lambda_0$ to $z = -2.25\lambda_0$ along the z axis. The region of interest is discretized into $21 \times 21 \times 21$ voxels. One builds the MSR matrix with the scatters placed in $\mathbf{r}_{m1} = (0.25\lambda_0, 0.12\lambda_0, -0.74\lambda_0)$ and $\mathbf{r}_{m2} = (-0.65\lambda_0, 0.32\lambda_0, -0.74\lambda_0)$, respectively.

A white Gaussian noise with signal to noise ratio SNR = 30 dB is injected into the scattered field measured at the receivers' position: this will simulate to some extent the noise which may perturb the acquisition of

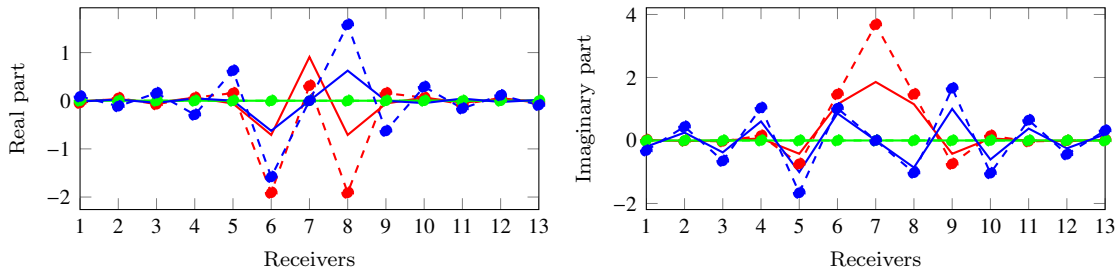

Fig. 3: Dipole along the x axis: E_x (— MoM, -•- asymptotic), E_y (— MoM, -•- asymptotic), E_z (— MoM, -•- asymptotic).

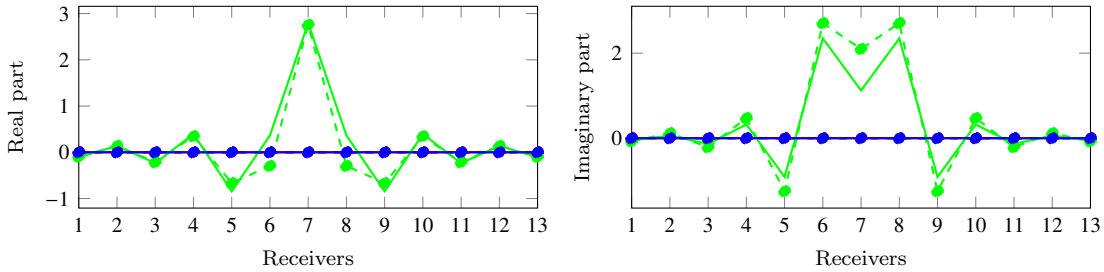

Fig. 4: Dipole along the y axis: E_x (— MoM, -•- asymptotic), E_y (— MoM, -•- asymptotic), E_z (— MoM, -•- asymptotic).

experimental data.. One of the key parameters of the MUSIC algorithm is the choice of the number of singular values s which is used to define the signal and the noise subspace. As exemplified in Fig. 6 the evolution of the amplitude of the singular values is typical of a classical L-curve which can be found in the regularized inversion techniques leading to the use of a corner detection method developed in such a framework (Hansen, Jensen, and Rodriguez 2007) to automatically estimate s. As shown in Fig. 6 such an approach seems to be efficient since it provides $s = 6$ which is the expected value for two defects.

The imaging through isosurface representation of the two scatterers is shown in Fig. 7. As one can notice first, the two scatterers are correctly spotted by the MUSIC with enhanced resolution whereas the standard MUSIC fails.

However, one can notice that such a representation does not provide a complete representation of the results obtained. Thus, the normalized full pseudo-spectrum representation of the two imaging functions is displayed in Fig. 8 and Fig. 9. By comparing those figures to Fig. 7 it appears that the pseudo-spectrum representation provides a better understanding of the results obtained.

4 Conclusion and perspectives

A method based on the first-order approximation to compute the electric field scattered by inclusions embedded in composite material (glass-fiber like) has been presented and validated. The Lippman-Schwinger equation based on the polarization tensor, which depends upon the geometrical shape of the inclusion, is exploited in harmony with the Padua-Domínguez interpolation-integration technique. Such a technique has been revealed to be effective to treat fast-oscillating spectrum, which may occur in imaging applications if one considers the emitting source far away with respect to the origin of the reference system. MUSIC with enhanced resolution turned out to provide imaging results of better quality with respect to the standard ones. The scenario presented in the numerical examples is still far from real-life application. Yet the implementation of the proposed method in multi-layer structures is straightforward. The implementation of the proposed method in the low frequency realm (eddy-current testing) is being investigated.

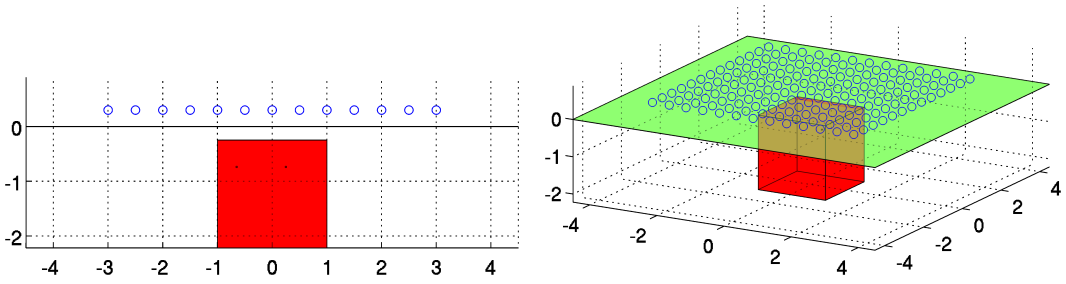

Fig. 5: Configuration for inverse imaging testing. Side view (left) and 3D view (right); $x, y, z/\lambda_0$.

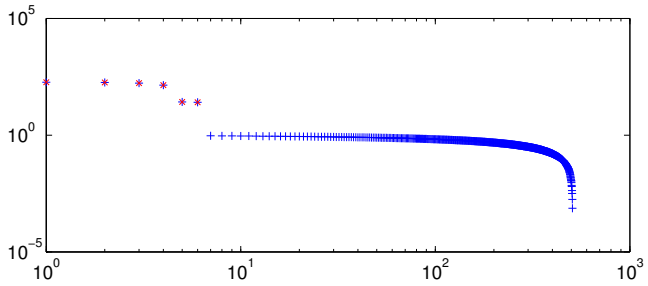

Fig. 6: Singular values obtained withe the 30 dB noise data. In red the s first values used to define the signal space.

5 Bibliography

Ammari, H., E. Iakovleva, D. Lesselier, and G. Perrusson (2007). "MUSIC-type electromagnetic imaging of a collection of small three-dimensional inclusions". *SIAM Journal of Scientific Computing* 29, pp. 674–709.

Caliari, M., S. De Marchi, A. Sommariva, and M. Vianello (2011). "Padua2DM: fast interpolation and cubature at the Padua points in Matlab/Octave". *Numerical Algorithms* 56, pp. 45–60.

Chen, X. and Y. Zhong (2009). "MUSIC electomagnetic imaging with enhanced resolution for small inclusion". *Inverse Problems* 25.

Domínguez, V., I. G. Graham, and V. P. Smyshlyaev (2011). "Stability and error estimates for Filon-Clenshaw-Curtis rules for highly oscillatory integrals". *IMA Journal of Numerical Analysis* 31, pp. 1253–1280.

Hansen, P. C., T. K. Jensen, and G. Rodriguez (2007). "An adaptive pruning algorithm for the discrete L-curve criterion". *Journal of Computational and Applied Mathematics* 198.2. Special Issue: Applied Computational Inverse Problems, pp. 483–492. ISSN: 0377-0427. DOI: `http://dx.doi.org/10.1016/j.cam.2005.09.026`. URL: `http://www.sciencedirect.com/science/article/pii/S0377042705007284`.

Henriksson, T., M. Lambert, and D. Lesselier (2011). "Non-iterative MUSIC-type algorithm for Eddy-current nondestructive evaluation of metal plates". *Electromagnetic Non-Destructive Evaluation,* T. Chady *et al.* eds, IOS Press, Amsterdam 14, pp. 22–29.

Iakovleva, E., S. Gdoura, D. Lesselier, and G. Perrusson (2007). "Multistatic response matrix of a 3-D inclusion in half space and MUSIC imaging". *IEEE Transactions on Antennas and Propagation* 55, pp. 2598–2609.

Sihvola, A. (2005). "Metamaterials and depolarization factors". *Progress In Electromagnetic Research, PIER* 51, pp. 65–82.

Teo, Y., X. Wang, and W. Chiu (2006). "Simulations of microwave propagation in delaminated unidirectional glass-epoxy laminate". *Composite Structures* 75, pp. 422–427.

Weiglhofer, W. S. and A. Lakhtakia (1996). "New expressions for depolarization dyadics in uniaxial dielectric-magnetic media". *International Journal of Infrared and Millimeter Waves* 17, pp. 1365–1367.

Zhong, Y., P.-P. Ding, M. Lambert, D. Lesselier, and X. Chen (2014). "Fast calculation of scattering by 3-D inhomogeneities in uniaxial multilayer, submitted to *IEEE Transactions on Antennas and Propagation*".

Zhong, Y., M. Lambert, D. Lesselier, and X. Chen (2014). "Electromagnetic response of anisotropic laminates to distributed sources". *IEEE Transactions on Antennas and Propagation* 62, pp. 247–256.

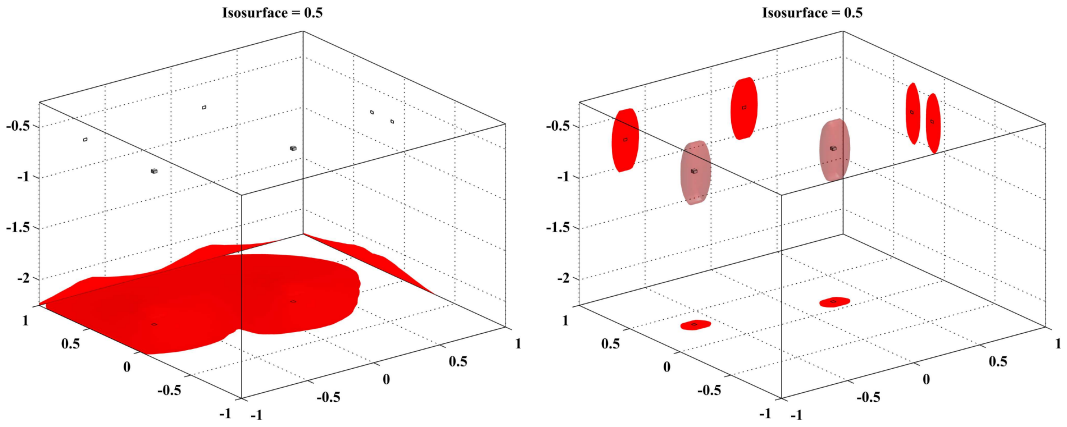

Fig. 7: Imaging results of two scatterers in the region of interest with 30 dB noise. Standard (left) and enhanced (right) MUSIC; $x, y, z/\lambda_0$.

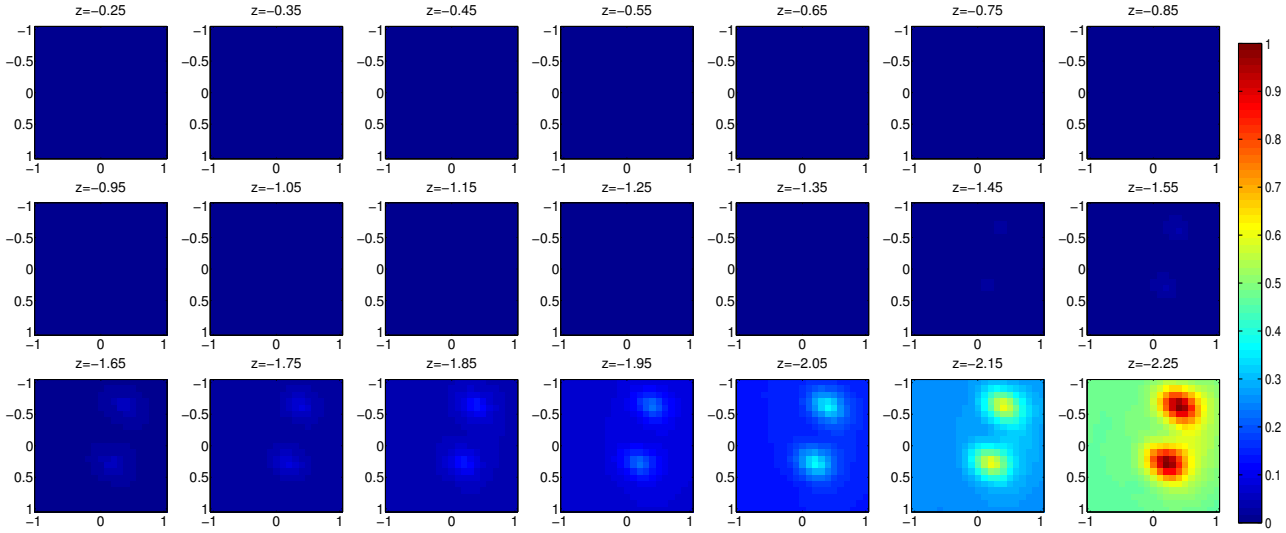

Fig. 8: Normalized spectrum of the imaging function corrupted with 30 dB noise. Standard MUSIC.

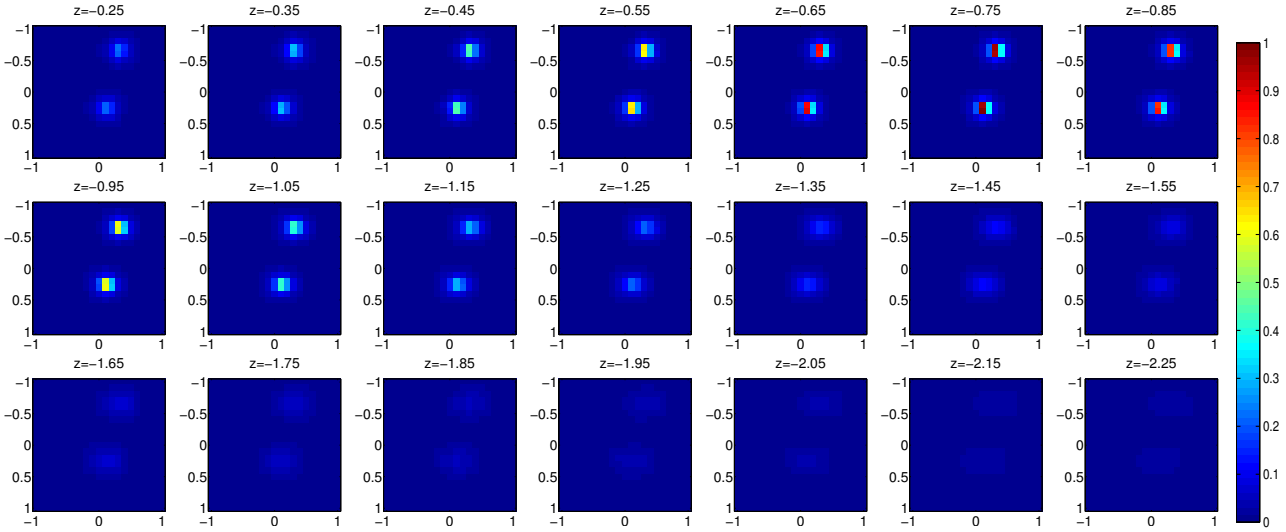

Fig. 9: Normalized spectrum of the imaging function corrupted with 30 dB noise. Enhanced MUSIC.